Available online at www.sciencedirect.com

ScienceDirect

Procedia Structural Integrity 68 (2025) 634–640

Structural Integrity Procedia

www.elsevier.com/locate/procedia

European Conference on Fracture 2024

Fatigue cracking in additively manufactured titanium aluminides

Mauro Filippini[a]*

[a]*Politecnico di Milano, Dipartimento di Meccanica, Via La Masa 1, 20156 Milano, Italy*

Abstract

Over the last decade, additive manufacturing technologies have been used to effectively produce gamma-TiAl alloys suitable for structural components. In this work, the fatigue crack growth properties of a high-Nb containing TiAl alloy (Ti-45Al-8Nb-2Cr) produced by additive manufacturing by Electron Beam Melting (EBM) technology is experimentally analyzed. Fatigue crack growth experiments with sub-size SENT specimens have been conducted with the aim of highlighting the behaviour of fatigue cracks in the threshold region of this TiAl alloy with fully lamellar microstructure. Compression pre-cracking procedure and subsequent fatigue crack growth tests with constant loading amplitudes are reported and compared with fatigue crack growth tests conducted with standard C(T) specimens. Experimentally measured crack closure levels and comparison with the roughness induced closure geometric model by Suresh, Ritchie (1982) provide information on the role of the coarse fully lamellar microstructure on the fatigue properties of TiAl alloys, in view of the application of TiAl intermetallics to structural components.

Keywords: fatigue crack propagation, intermetallic alloys, crack closure, fatigue thresholds

1. Introduction

Gamma titanium aluminide-based alloys are considered more and more as a potential substitute of the currently employed nickel superalloys for structural applications in the aeroengines industry, as the material of choice for low-pressure turbine blades, Appel (2011), Leyens (2003). Development and advancement of gamma titanium aluminides technologies is regarded as a key factor of competitive advantage for achieving the targets of improvement of the

* Corresponding author. Tel.: +39-02-2399-8220.
E-mail address: mauro.filippini@polimi.it

10.1016/j.prostr.2025.06.108

engine efficiency, of reduction of carbon dioxide emissions and for opening the design space to a new generation of gas turbine engines, Bewlay (2016). In the last decade, additive manufacturing technologies, remarkably those based on selective powder bed fusion, have proved to be key enabling technologies in many industrial sectors, especially where geometrical complexity of the mechanical components or the technical limitations in the use of highly specialized materials do not allow the application of consolidated, conventional technologies. Additive manufacturing by Electron Beam Melting (EBM) may be used to effectively produce gamma titanium aluminide (TiAl) intermetallic alloys with mechanical properties suitable for structural components, Biamino (2011). TiAl alloys offer the advantage of favorable specific strength, also at moderately high temperatures, and they are now considered as a potential substitute of the currently employed alloys in some specific applications in the energy, aerospace, and automotive industry (e.g., turbochargers wheels and engine valves), Clemens (2013). Even if TiAl alloys provide favourable specific strength at the relevant temperatures compared to competing nickel superalloys, they're regarded as more complex to design components with, due to their limited fracture toughness and strain at failure compared with conventional alloys, especially at room temperature. Moreover, depending on their final microstructure, fatigue strength is one of the most important design requirements, in the view of designing structural parts.

In this work, the fatigue crack growth properties of a high-Nb containing TiAl alloy (Ti-45Al-8Nb-2Cr, at. %) produced by additive manufacturing by Electron Beam Melting (EBM) technology is experimentally analysed. Fatigue crack growth experiments with sub-size SENT specimens have been conducted with the aim of highlighting the mechanical behaviour and the interaction with the microstructure of fatigue cracks in the threshold region of this TiAl alloy, with special focus to the contribution of shielding mechanisms and crack closure in the near threshold regime.

2. Material and specimen design

2.1. Material

The gamma titanium aluminide (γ-TiAl) Ti-45Al-8Nb-2Cr (at. %) intermetallic alloy studied in this work was produced by powder bed fusion additive manufacturing technique by electron beam melting (EBM), by means of the EBM A2 machine manufactured and distributed by ARCAM AB (Sweden). The higher niobium content of this chemical composition increases the oxidation resistance at high temperature compared to other alloys (e.g., Ti-48Al-2Nb-2Cr), Terner (2012). After EBM, the as-built material produced in a cuboidal shape undergo hot isostatic pressing (HIPing), as described also in Biamino (2011) and subsequent heat treatment; depending on the heat treatment temperatures, fully lamellar or duplex microstructures may be obtained. Further details on processing and monotonic properties are given by Terner (2012). In the case of the material studied in the present work, final microstructure is predominantly made by lamellar grains with grain size ranging from 200 to 500 μm, with an average grain size of about 300 μm, as shown in Fig. 1.

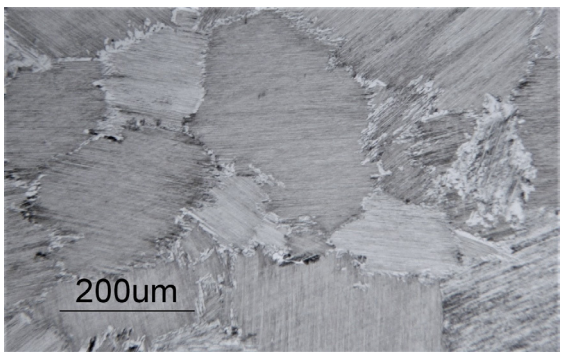

Fig. 1. Ti-45Al-8Nb-2Cr: near-fully lamellar microstructure after heat treatment. Heat treatment details in Terner (2012).

2.2. Specimen design and pre-cracking

The samples were cut by wire Electro-Discharge Machining (EDM) out of 2 in wide and 1 in thick C(T) specimens that were left over from a previous test campaign in the form of 4 small squared-section block (12x12 mm cross section, 28 mm height), with the shape shown in Fig. 2. For each block, at mid-height, a deep notch with a depth of 4.60 mm and a tip radius of about 150 µm was manufactured by thin wire EDM, so that fatigue cracks can be generated at the notch root by employing a specific procedure.

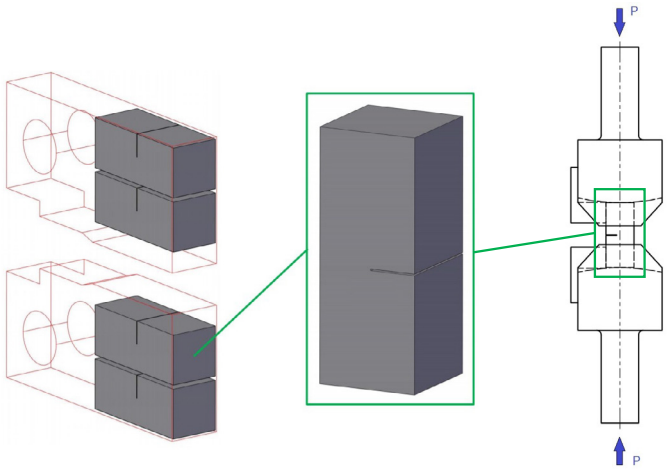

Fig. 2. Starter block (SENT) specimens and cyclic compression pre-cracking.

Due to the peculiar mechanical properties of TiAl intermetallic alloys, it's been proved that the most suitable method for initiating fatigue cracks for subsequent fatigue crack growth tests is given by compression pre-cracking, as shown by Pippan (2001), and Eck et al (2020). Compression pre-cracking has been applied to the small block specimens by employing a specially designed gripping device, as shown in Fig. 2. The cyclic loading in compression is applied to the notched small block specimens along the center load line by means of two opposing cylindrical surfaces with a suitable radius, by applying opposite forces acting on the upper and lower surfaces of the specimens. The positioning of the specimens prior to the compression pre-cracking is ensured by lateral flat surfaces. During the compression pre-cracking procedures, it has been observed that a minimum (compressive) force is sufficient to keep the specimens in place. The cyclic compressive loading was applied to the specimens with a loading ratio $R=F_{min}/F_{max}=10$, so that for a notch depth of 4.60 mm a stress intensity factor range ΔK in the range 15–18 MPa $\sqrt{m}$ has been applied during pre-cracking. The stress intensity factor was calculated by employing the configuration correction factors for SIF given by Tada (2000) and Huang (2018). By compression pre-cracking, cracks are generated at the notch tip as in the case of the crack initiation in cyclic tension but, with the advantage that once cracks are initiated, their growth tend to decrease progressively until they stop propagating, Tabernig (2002). The typical initial cracks emanating from the starter notch tip are shown in Fig. 3. It should be observed that multiple cracks may appear, or no cracks are observable at the lateral surfaces, due to the specific orientation of lamellar colonies respect in the vicinity of the notch. However, based on results obtained in previous fatigue experiments with other variants of TiAl alloys, it's been decided to proceed cutting the final SENT specimens from the pre-cracked starter blocks.

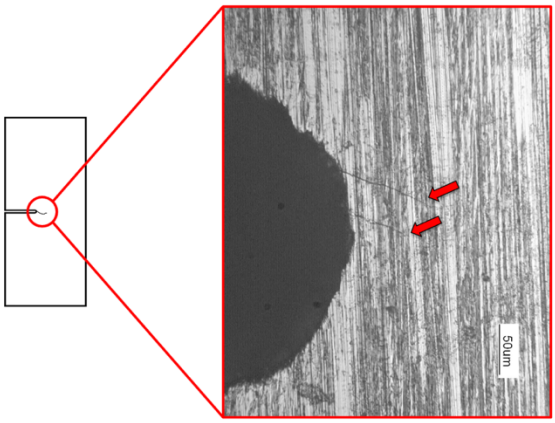

Fig. 3. Pre-cracks initiated by compression pre-cracking out of the starter notch.

The final size and dimensions of the sub-size SENT specimens is shown in Fig. 4. The specimens were cut by EDM out of the pre-cracked starter blocks, by removing a layer of 1 mm from both lateral surfaces and by vertical cutting the starter blocks by wire EDM with a wire diameter of 0.5 mm. For each of the 4 starter blocks, 3 specimens with a thickness of 3 mm each has been obtained. Symmetric beveled holes have been cut on the specimen axis, so that specimen could be loaded in tension by mean of a specifically designed and manufactured set of clevis grips. Prior to testing, the lateral surfaces of the SENT specimens have been mirror-polished by abrasive papers and diamond paste and then chemically etched by swabbing, to reveal the size and orientation of the pre-cracks respect to the microstructure in the vicinity of the notch.

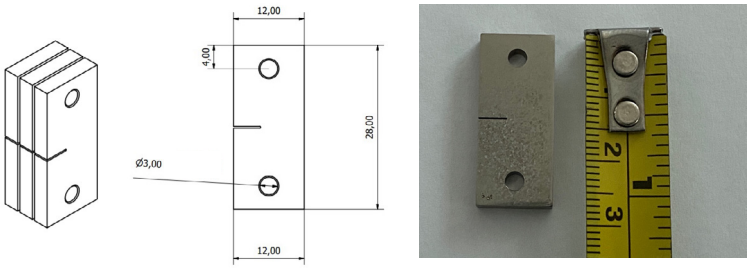

Fig. 4. Sub-size SENT specimen employed for the fatigue crack growth tests.

3. Fatigue crack growth tests

Fatigue crack propagation tests have been performed by employing a servo-hydraulic MTS 810 test system available in the laboratories of the Department of Mechanical Engineering of Politecnico di Milano. A set of custom clevis grips was designed and manufactured, so that the sub-size SENT could be loaded in tension. Special care has been taken to avoid introducing lateral bending and load misalignment. For this reason, the clevis grips have been connected to the load cell and to the test system actuator through spherical joints.

In conducting the tests, recommendations given by the ASTM E647 standard have been followed as far as possible, considering the size and the shape of the sub-size SENT specimens. However, due to the lack of access space, it was not possible to directly monitor the evolution of the crack length during the fatigue crack growth tests by using a clip-on-gauge extensometer. For that reason, fatigue tests have been stopped after a programmed number of loading cycles, the crack length on both lateral surfaces measured by mean of an optical microscope and fatigue tests restarted for the subsequent steps.

Fatigue crack growth tests have been conducted on 8 of the 12 manufactured specimens, so that 4 specimens remain available for future experiments and analysis. Fatigue tests have been performed with constant load range throughout each test, with a frequency of 20 s^{-1} and loading ratio R=0.05. Experimentally measured fatigue crack growth rates da/dN are reported in Fig. 5 and compared with test results obtained in previous fatigue test conducted on high-Nb alloys with standard C(T) specimens (W=1 in=25.4 mm; B=0.5 in).

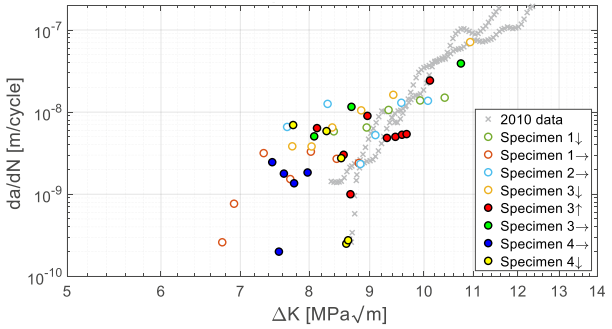

Fig. 5. Fatigue crack growth rate da/dN vs applied ΔK (R=0.05). Comparison with data obtained with standard specimen.

The initial fatigue loading conditions were set based on previous tests, so that (initial) applied ΔK in the first loading step was just above the fatigue threshold ΔKth. The optically measured crack length is used for the calculation of the average crack growth rate da/dN according to the incremental polynomial method, as recommended by ASTM E 647 standard. In Fig. 5, the open dots refer to microstructurally short cracks that are in proximity of the notch tip, while full dots represent da/dN values of cracks extending into the material and crossing several grains.

As the crack propagates and the applied ΔK increases under constant cyclic loading condition, as the tests progressed, the fatigue test were stopped and restarted more frequently, so that the final crack length did not exceed a target final length. Out of the 4 performed fatigue tests, one specimen failed after 105900 loading cycles when crack propagation resulted in an applied K_{max} above 12-14 MPa √ m. The remaining fatigue tests were stopped before specimen failure, with applied ΔK still below 10 MPa √ m in the last step of the fatigue test.

The evolution of the fatigue cracks was observed by optical microscope observations, allowing to reconstruct the progressive interaction of the growing cracks with the microstructure, as it shown in Fig. 6.

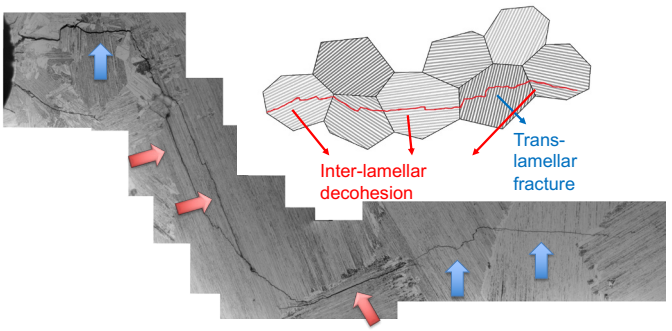

Fig. 6. Observation of growing cracks in TiAl alloys and interaction with microstructure features.

In the 2D view of the crack propagation as observable on the lateral surfaces of the specimens, it can be observed that fatigue accumulation damage is governed by the local microstructure, Patriarca (2016), and crack path is heavily controlled by the orientation of lamellar grains respect to the main loading direction and the crack propagation direction, resulting in a complex zig-zag pattern. In general, in the early stages of crack propagation in the proximity of the notch tip, cracks tend to growth by interlamellar decohesion, by propagating along the main direction of

lamellae. As the cracks extend into the material, and the stress intensity factor increases, the available energy may become sufficient to activate the trans-lamellar crack propagation mechanisms. As a result, the cracks tend to propagate in normal direction respect to the applied loading. However, when growing cracks cross lamellar grain that are not excessively misaligned with respect to the direction normal to the loading, the inter-lamellar decohesion is likely to be the main fracture mechanism.

4. Crack closure mechanisms

By the observation made on propagating cracks, it became evident that a certain amount of crack deflection is always present, as the propagation direction usually changes when the fatigue cracks cross lamellar grains with different orientations. This phenomenon results in relatively rough fracture surfaces, with the premature contact between the fracture surface asperities during the unloading phase of the fatigue cycle, suggesting that roughness induced closure may play an important role in the fatigue damage process. For this reason, by using a subset of the sub-size specimens, crack closure levels have been experimentally measured by applying the compliance offset method, ASTM E 647. The closure measurement tests were carried out under force control using an electro-mechanical MTS testing machine under quasi-static loading. Each specimen was submitted to five loading cycles with a minimum and maximum load of respectively 100 N and 1000 N. The crack mouth opening displacement was monitored by using an MTS compact extensometer (gauge length 8 mm, resolution 10-6 mm). The application of such extensometer was made possible from the quasi-static nature of closure measurement tests.

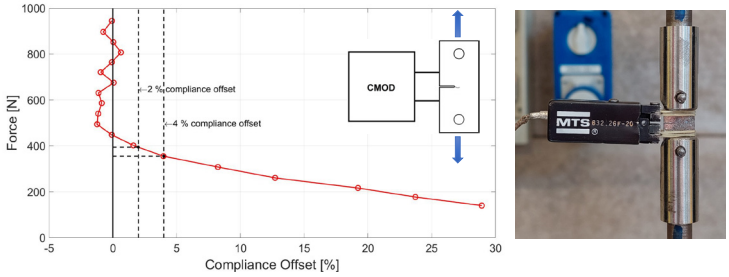

Fig. 7. Crack closure levels measured by applying the compliance offset method, ASTM E 647.

The crack length measured by the compliance method by the extensometer measurement according to the ASTM E 647 standard was crosschecked against the optical measurements of the crack length. Then by applying the data analysis procedure illustrated in the ASTM E 647 standard the closure levels were measured, as it's shown in Fig. 7. However, in some of the tests, the acquired data did not meet the requirements of the standard. Thus, the crack closure level could be assessed for some of the specimens tested, with measured ratios of K_{cl}/K_{max} equal ranging from about 30% to about 40%.

In order to model the roughness induced closure phenomenon, the micro-geometric model of Suresh, Ritchie (1982) was applied. The application of the model requires to identify the average ratio h/w of the height h and width w of the crack asperities by manually digitizing the crack profile. In the tested specimens the measured h/w range from about 0.15 to about 0.25. In Figure 8, the comparison of the prediction of the closure levels K_{cl}/K_{max} given by the Suresh-Ritchie and the values measured by the compliance offset method is reported. The shaded area represents the prediction of the model when the mode II displacement is varied between 1.5 and 3 µm, while the dots represent the closure levels measured compliance offset method. Assuming that the Suresh-Ritchie model provides sufficiently accurate results, a major component of the closure effect (between 70% and 85%) can be attributed to the roughness of the fracture surfaces.

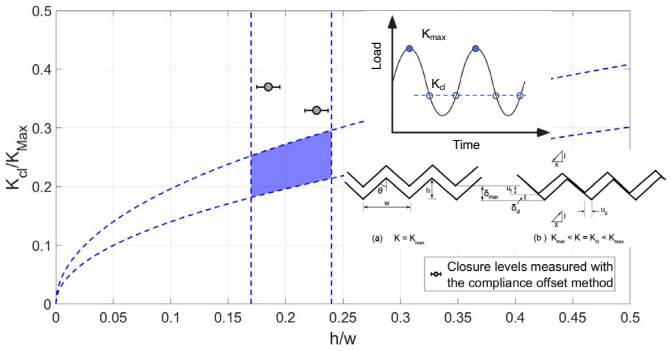

Fig. 8. Crack closure modelling. Comparison of crack closure levels measured.

5. Conclusion

The crack propagation rates measured within the miniaturized SENT specimens are consistent with the data previously collected with standard C(T) specimens, giving confidence that the present test technique could be applied extensively for assessing the fatigue properties of TiAl alloys, especially when limited quantity of material is available for testing. The lamellar microstructure is responsible for different "apparent" strengthening mechanisms, such as bridging, crack deflection, crack branching and microcrack shielding. However, in the case of the studied microstructure, fatigue cracks are allowed propagating as short cracks for longer distances, due to the relatively large grain size. The intensity of the closure phenomenon is remarkable, as can be observed from the opening forces. According to the Suresh-Ritchie model a significant part of the closure phenomenon can be attributed to roughness-induced closure. Future activities will require to acquire more data on crack propagation and especially on the contact between fracture surface asperities, which is responsible for roughness-induced closure. More refined crack closure model(s) will provide more reliable closure levels assessment and allow to identify the correct stress intensity threshold $\Delta K_{th,eff}$ for the fatigue design of mechanical structural components.

References

Appel, F., Paul, J. D. H., Oehring, M., 2011. Gamma titanium aluminide alloys: science and technology. John Wiley & Sons.

Leyens, C., Peters, M. (Eds), 2003. Titanium and Titanium Alloys, WILEY-VCH.

Bewlay, B.P., Nag, S., Suzuki, A., Weimer, M. J., 2016. TiAl alloys in commercial aircraft engines. Mater. High Temp., 33(4-5), 549–559.

Biamino, S., Penna, A., Ackelid, U., Sabbadini, S., Tassa, O., Fino, P., Pavese, M., Gennaro, P., Badini, C., 2011. Electron beam melting of Ti-48Al-2Cr-2Nb alloy: microstructure and mechanical properties investigation. Intermetallics, 19(6), 776-81.

Clemens, H., Mayer, S., 2013. Design, Processing, Microstructure, Properties, and Applications of Advanced Intermetallic TiAl Alloys. Advanced Engineering Materials, 15(4), 191–215.

Terner, M., Biamino, S., Penna, A., et al., 2012. Material properties of TiAl alloy with high Nb content produced by the additive manufacturing technology of Electron Beam Melting. EuroPM 2012 Conference, Vol. 1: PM Applications and new processes.

Pippan, R., Hageneder, P., Knabl, W., Clemens, H., Hebesberger, T., Tabernig, B., 2001. Fatigue threshold and crack propagation in gamma-TiAl sheets. Intermetallics, 9(1), 89–96 (2001).

Eck, S., Maierhofer, J., Tritremmel, C., Gaenser, H. P., Marsoner, S., Martin, N., Pippan, R., 2020. Fatigue crack threshold analysis of TiAl SENT and CC specimens – Influence of starter notch and precracking. Intermetallics, 121, 1067–70.

Tada, H., Paris, P. C., Irwin, G. W., 2000. The Stress Analysis of Cracks Handbook, 3rd ed., ASME Press, New York.

Huang, Y., Zhou, W., 2018. Stress intensity factor for clamped SENT specimen containing non-straight crack front and side grooves. Theoretical and Applied Fracture Mechanics, 93, 116 – 127.

Tabernig, B., Pippan, R., 2002. Determination of the length dependence of the threshold for fatigue crack propagation. Engineering Fracture Mechanics, 69(5), 899–907.

ASTM E 647, Standard Test Method for Measurement of Fatigue Crack Growth Rates, ASTM International.

Patriarca, L., Filippini, M., Beretta, S., 2016. Digital image correlation-based analysis of strain accumulation on a duplex gamma-TiAl, Intermetallics, 75, 42–50.

Suresh, S., Ritchie, R.O., 1982. A Geometric Model for Fatigue Crack Closure Induced by Fracture Surface Roughness. Metall Trans A, 13(9), 1627–1631.